On the Use of Meta-Signals to Counteract Ionospheric Phase Advance Effects on Wideband LEO PNT Signals

(Article begins on next page)

30 April 2024

On the Use of Meta-Signals to Counteract Ionospheric Phase Advance Effects on Wideband LEO PNT Signals

Alex Minetto ⓘ, Andrea Nardin ⓘ, Fabio Dovis ⓘ, *Politecnico di Torino, Turin, Italy*

BIOGRAPHY

Alex Minetto received the M.sc. degrees in Telecommunications Engineering from Politecnico di Torino, Turin, Italy and his Ph.D. degree in Electrical, Electronics and Communications Engineering, in 2020. He joined the Department of Electronics and Telecommunications of Politecnico di Torino in 2021 as researcher and assistant professor. His current research interests cover navigation signal design and processing, advanced Bayesian estimation applied to Positioning and Navigation Technologies (PNT) and applied Global Navigation Satellite System (GNSS) to space weather and space PNT.

Andrea Nardin received the M.Sc. degree in Telecommunications engineering and the Ph.D. degree in Electrical, Electronics and Communications Engineering, in 2018 and 2023, respectively, both from Politecnico di Torino, where he is currently a postdoctoral researcher. From 2018, he has been working on satellite navigation technologies with the Navigation Signal Analysis and Simulation (NavSAS) group at Politecnico di Torino and in 2021 he was a Visiting Doctoral Researcher at Northeastern University, Boston, MA, USA with the Information Processing Lab (IPL).

Fabio Dovis received his M.Sc. degree in 1996 and his Ph.D. degree in 2000, both from Politecnico di Torino, Turin, Italy. He joined the Department of Electronics and Telecommunications of Politecnico di Torino as an assistant professor in 2004 and as associate professor in 2014. Since 2021 he is a full professor. He coordinates the Navigation Signal Analysis and Simulation (NavSAS) research group. His research interests cover the design of GPS and Galileo receivers, advanced signal processing for interference and multipath detection and mitigation, as well as ionospheric monitoring.

ABSTRACT

The recent, massive deployment of Low-Earth Orbit (LEO) satellites constellations for broadband communication services is attracting the attention of the Positioning, Navigation and Timing (PNT) community concerning the possibility of complementing current Global Navigation Satellite System (GNSS) through LEO radionavigation signals. Motivated by lower free-space path loss brought in by smaller orbital radia, legacy radionavigation frequency bands as well as less congested bands such as S, C, X, Ka and Ku could host dedicated radionavigation signals or combined solutions that hybridize them with communications signals. However, as per current GNSS signals, LEO radionavigation counterparts will still suffer the effects of intense ionospheric activity. In particular, in spite of higher carrier frequencies which limit the impact of their interaction with the ionosphere, non-negligible ionospheric-induced phase advance has the potential of impoverishing the correlation performance of wideband modulation schemes that may be intrinsically of interest in the design of wide and ultra-wideband navigation signals from LEO. Building on insights from previous literature on Galileo wideband signals and their interactions with ionosphere, we analyze the dispersive effect of the ionosphere on a sample wideband channel of 128 MHz hosting signals with different modulations. We then propose the use of metasignals to overcome the limitation of native wideband signals such as high-order Binary Offset Carrier modulations. The results demonstrate that simplistic BPSK-based meta-signals can be designed to be more robust than wideband BPSK modulations and bandwidth-equivalent BOC signals.

I. INTRODUCTION

As the demand for precise and reliable GNSS continues to grow, Low-Earth Orbit (LEO) satellites have gained prominence in the field due to their current usage in broadband communication systems. However, as per their Medium-Earth Orbit (MEO) counterparts, radio navigation signals from LEO satellites are susceptible to ionospheric effects, especially for large bandwidth occupations, which can significantly degrade positioning accuracy. In particular, ionospheric activity is responsible for two detrimental signal impairments, i.e., the group delay and the phase advance, degrading GNSS performance. They respectively induce non-negligible i) pseudorange bias and ii) correlation impoverishment at the receiver, and their magnitude inversely depends on the transmitted signal carrier frequency and directly on the ionospheric Total Electron Content (TEC). (Hoque et al., 2017). Group delay is typically compensated at the receiver through modeling and correction techniques (Kindervatter and Teixeira, 2022). Furthermore, dual-frequency GNSS receivers almost neutralize the impact of this effect on the estimation of pseudorange measurements by leveraging the so-called iono-free measurements. Differently, phase advance has been assumed

negligible in current satellite radio-navigation systems, in light of the flat phase response of the transionospheric channel for state-of-the-art GNSS narrowband signals. However, as far as the nominal signal bandwidth is expected to expand in LEO systems, the phase advance may cause severe signal distortion at high TEC values, thus leading to non-negligible correlation losses. Such a loss may degrade the correlation performance of modern signal architectures such as Binary Offset Carrier (BOC) modulations conceived for high-accuracy services, thus causing reduced acquisition sensitivity and possible instability of the tracking loops. Such a distortion and related effects were discussed as a major concern for Galileo wideband signals (Gao et al., 2007). The study concluded that wideband or ultra-wideband, transionospheric radio-navigation signals would never be a robust choice in future GNSS systems due to the potential correlation drop they may face at high TEC values. Besides, the authors suggested the use of narrower subbands to counteract this impairment. Recently, this limitation has been revised and further analyzed for Galileo E5 AltBOC(15, 10) and Beidou BDS B3 BOC(15, 2.5) (Zhao and Lei, 2023). As far as the interest towards ultra-wide-band signals grows, along with the usability of higher frequency bands such as S, C, X, Ku, and Ka, this concern has to be extended and revised across these frequency ranges, as the ionospheric phase advance may still reduce the performance of advanced modulation schemes despite the high carrier frequencies. In fact, at these carrier frequencies, large channels of hundreds of MHz can be exploited for both communication and radio-navigation.

Recently, the joint processing of synchronous GNSS signals received at different frequencies has been exploited to achieve improved code estimation accuracy (Paonni et al., 2014; Borio and Gioia, 2023; Gao et al., 2020). This approach is often regarded as meta-signal processing. It is noteworthy that so-intended meta-signals do not inherently embody a conventional signal subcarrier modulation technique. Nevertheless, the treatment of these components as a singular signal can present an analogous scenario to the observation of a subcarrier with specific subchip shaping characteristics. Meta-signals allow for achieving the advantages of wideband signals by combining narrowband signal components (Paonni et al., 2014; Nardin et al., 2020a) which may be intrinsically less susceptible to the ionospheric phase advance (Gao et al., 2007). In light of this, meta-signals represent a suitable solution for high-accuracy, ultra-wide-band radio-navigation in the upcoming LEO PNT systems at the cost of an increased receiver complexity (Nardin et al., 2020b, 2021). These advantages especially hold for those bands in which wide-band and ultra-wideband signals can be heavily degraded by intense ionospheric activity. By following the introduction of its basic principles, the processing of meta-signals has been investigated adopting different receiver architectures and concepts, both leveraging GNSS signal components transmitted over different carrier frequencies (Borio and Gioia, 2023; Gao et al., 2020) and generalizing the concept to other types of signal orthogonality, i.e. jointly processing signal components that can be transmitted over the same carrier frequency (Nardin et al., 2021). Meta-signals have been also investigated with respect to several impairments. They have been recently studied for mitigating multipath effects (Chang et al., 2022) and to assess the impact on their correlation properties of non-ideal propagation phenomena, such as attenuation and group delay (Nardin et al., 2020a). An extended analysis focused on ionospheric effects and involving phase advance is, however, missing in the current literature, while meta-signals applications in this domain are already of practical interest. While acknowledging potential formal ambiguities, in the following we may occasionally refer to the proposed meta-signal architecture as one of the investigated subcarrier modulation schemes.

This study first highlights the effect of ionospheric phase advancement on a set of wideband signal modulations conceived to fit LEO PNT operational bandwidths (including also legacy Radio Navigation Satellite Services (RNSS) lower bands for completeness). Besides, it proposes Binary Phase Shift Keying (BPSK)-based meta-signals to overcome the dispersive effect of the ionosphere while still preserving the advantage of wideband radio-navigation, as a wideband coupling of narrowband signals transmitted over different carriers with a given frequency spacing (Nardin et al., 2021).

The remainder of this paper unfolds as follows: Section II initially introduces the notion of wideband radionavigation signals and subsequently outlines their interaction with the ionosphere. In Section III, we delve into the specifics of signal selection and design, the analytical simulation of ionospheric effects, and outline the methodology for three distinct analyses. Section IV showcases and discusses the outcomes of our investigations. Finally, in Section V, we draw conclusions based on the findings presented.

II. BACKGROUND

1. Wideband radionavigation signals

Wideband radionavigation signals for code ranging applications have been conceived since a long time. However, for both historical and technical reasons they have been disregarded for civil applications until modern receiver architectures. As an example, Galileo E6 Public Regulated Service (PRS) can be considered as a non-civil, wideband signal if compared with narrowband, civil counterparts at both GPS L1/L2 and Galileo E1 bands. For what concerns civil signals, the joint processing of E5a and E5b at Galileo E5 band could naturally lead to a wideband navigation signal recommended to be received with a 51.150 MHz bandwidth. However, its practical exploitation still faces a difficult market penetration in terrestrial GNSS receivers (Diessongo et al., 2012).

Recently, wideband or ultra-wideband radionavigation signals has regained attention along with the advent of LEO mega-

constellations to be put beside or complemented with broadband communication signals (Ries et al., 2023; García-Molina et al., 2023; Egea-Roca et al., 2021). To pursue an efficient usage of possible wideband and ultra-wideband channels primarily conceived for broadband satellites communications, the design of candidate PNT signals is expected to address two main aspects and extensive performance trade-offs:

- the signal main spectral lobe/lobes bandwidth which depends on the chip rate R_c of the ranging code and

- the subcarrier design which corresponds to the chip shape of the primary spreading code.

By fixing the primary code chip rate R_c, a proper choice of the subcarrier modulation scheme allows for an efficient channel usage in the sense of the Gabor bandwidth, thus spreading the signal power towards the boundaries of the present channel. This concept is related to the minimization of the Cramér–Rao bound (CRB) of a time-delay estimator and is leveraged by meta-signals thanks to the sideband components' frequency separation.

Any signal which is modulated by subcarriers that count a finite number of subchips can be described in the frequency domain f, through the generalized Fourier transform (Ávila Rodríguez, 2008)

$$S(f) = e^{-\frac{j\pi f}{nR_c}} \frac{\sin\left(\frac{\pi f}{nR_c}\right)}{\pi f} \sum_{i=1}^{n} s_i e^{j2\pi fi/nR_c} \tag{1}$$

where n refers to the number of subchip segments in a chip, s_i is the value assumed by the i-th subcarrier subchip, and R_c is the chip rate of the signal. In this paper we will make use of (1) for the construction of wideband BPSK, BOC, and also for meta-signals, as detailed in Section III.

2. Ionospheric modelling

Ionosphere is a dispersive medium that induces group delay and phase advance effects depending on the signal frequency and on the TEC of the ionospheric volume crossed by the signals. TEC variations can result from complex interactions among several factors and events, e.g., solar and geomagnetic activity, seasonal and daily changes, as well as earthquakes, eruptions and rocket launches. Group delay can be compensated by means of consolidated multi-frequency iono-free combinations (Imel, 1994) while phase advance would require a more advanced knowledge of the channel. Given that the two effects have the same magnitude but opposite sign, first and higher order ionospheric delay models can be considered to accurately characterise and quantify also the phase advance affecting wideband signals at different frequencies and TEC values. Although the first-order term represents the 99% of the overall contribution (Gao et al., 2007; Hoque and Jakowski, 2012), the current study also includes second and third order terms for the sake of completeness.

In this work, we assume future-proof high-accuracy services offered through wideband LEO radionavigation signals over a wide range of potential bands. In order to condition the received signal with ionospheric phase advance, the ionospheric transfer function is modelled according to

$$H_I(f, TEC) = e^{-j2\pi f \tau(f, \text{TEC})/c} \tag{2}$$

where f is the signal carrier frequency in Hz, c is the speed of light expressed in m/s, and $\Delta\tau = \sum_{i=1}^{3} \tau_i(f, \text{TEC})$ is the group delay expressed in seconds and approximated by the truncated sum of the following terms (Hoque et al., 2017):

- First-order term

$$\Delta\tau_1 = 40.3 \cdot \text{TEC}/f^2 \tag{3}$$

- Second-order term

$$\Delta\tau_2 = 11.28 \cdot 10^7 \cdot \text{TEC}/f^3 \tag{4}$$

- Third-order term

$$\Delta\tau_3 = 1602.81 \cdot N_m + 2.37 \cdot 10^{1}4 \cdot \text{TEC}/f^4 \tag{5}$$

where $N_m = \text{vTEC}/4.13h$ is the maximum electron density along the Line-of-Sight (LOS) between satellite and receiver (Pireaux et al., 2010) and depends on the vertical TEC (vTEC) and on $h = 7 \cdot 10^3$ m, which is the atmospheric scale height. The vTEC is measured in TEC units (TECu) and may vary between 1 TECu = $10^1 6$ el/m^2 and 300 TECu depending on a number of factors such as local time, geographic/geomagnetic location, season, solar activity level, etc.

It is worth remarking that this model does not account for path loss attenuation or for additional absorption effects causing selective attenuation across different frequencies that may be proper of the ionosphere. The present study solely focus on dispersive effects. It is also worth recalling that, by definition, group delay is opposite in sign w.r.t. the phase advance. Therefore, if signals are delayed by a group delay of $\tau(f)$,s the phase of each frequency component will be advanced of $-\tau(f)$,

according to their respective frequency components. In light of this, only the value of $\tau(f)$ is shown and discussed hereafter for simplicity. Fig. 1 shows the trend of $\tau \cdot c$ across the different bands of interests and for different sample values of TEC.
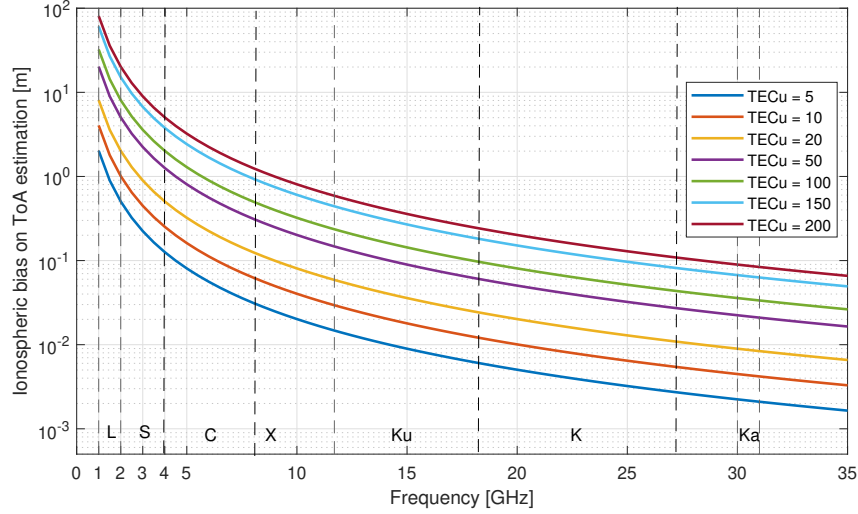

Figure 1: Trend of the ionospheric delay observed in the frequency interval $1 - 35$ GHz for different values of TEC.

Nominal TEC values hystorically showed nominal fluctuations between 0 and 100 TECu (Perevalova et al., 2008), however intense ionospheric activities raised up this value over 150 TECu (Ya'acob et al., 2019). In line with these, we assumed a large span of TEC values that describe a comprehensive range of intensities, thus spanning from quiet to severe ionospheric activity.

It is well known that τ decreases with frequency. This aspect makes the ionospheric impact more severe at lower frequencies. However, although ionosphere mostly affect low-frequency bands, the commonplace narrowband nature of the GNSS signals has typically led to neglect the phase advance impact in conventional GNSS signal processing. However it is fundamental to notice that wideband signals carried at frequencies higher than those in the L-band may still experience a non-negligible gradient of τ across their useful bandwidth which may degrade correlation properties.

As highlighted in (Gao et al., 2007) indeed, the delay exhibits neither constancy nor linearity across the frequency spectrum, and additionally, it is affected by evident asymmetry w.r.t. to a given center frequency. Due to this gradient, the different frequency components of a transionospheric signal do not maintain their relative phase relationships as they propagate through the channel, thus causing distortion.

3. Ionospheric effects on wideband signals

If wideband signals are targeted for the design of transionospheric navigation signals, the effects of phase advances must be considered among the sources of potential correlation loss. This aspect is often disregarded in signal design literature (Ji et al., 2021). In fact, by its nature, the ionospheric transfer function defined in (2) does not subtend distortions in the amplitude spectrum of the signal, however its effect on the different frequency components' phase introduces non-negligible distortions that potentially cause

- ripples in the time-domain signal,
- power loss and asymmetry of the correlation peak,
- phase fluctuations in the Phase-Lock Loop (PLL) output.

Fig. 2 shows the effect of both group delay and phase advance experienced by a wideband BOC-modulated signal carried at $f_c = 1176.45$ MHz and crossing the ionosphere with TEC = 10 TECU. By looking at Fig. 2a we can notice that signal's Power Spectral Density (PSD) do not present alterations. Differently, in Fig. 2b, the comparison of the iono-free signal (black) and iono-affected components (red) highlights a severe distortion of the chip shape which is characterized by i) a phase rotation of the iono-affected signals, ii) smoother rising edges, iii) remarkable fluctuations of the sub-chip amplitude, and iv) a poor symmetry of the overall chip shape.

We remind that Gibbs phenomena affecting the iono-free signal in Fig. 2b are due to the finite nature of the processing, as in the case of inverse FFT applied to the analytic formula for computing the time-domain shaping of the signal. Details about this

methodology are clarified later in the manuscript. It is also worth noticing that despite the generated sequence was purely real
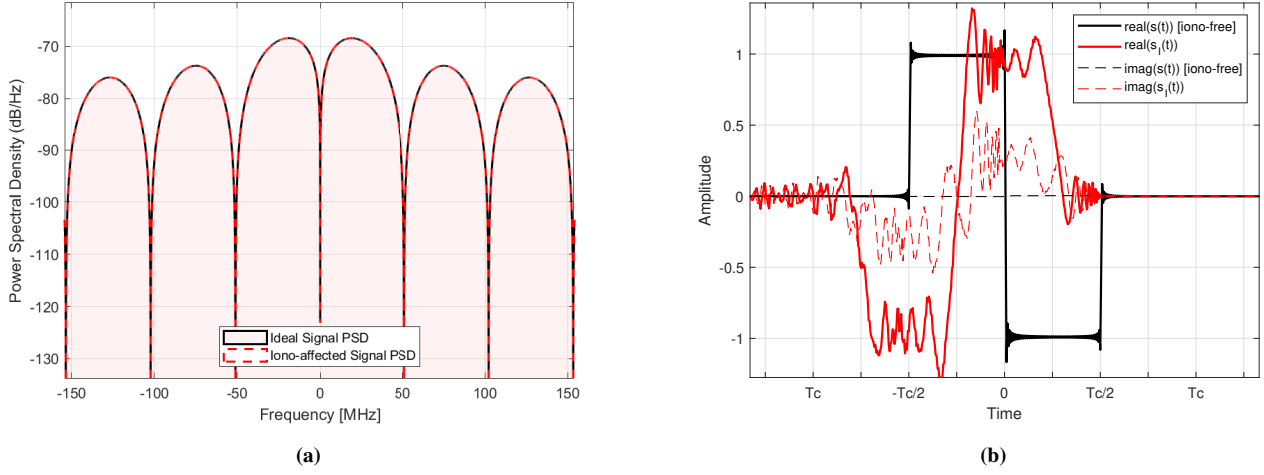

Figure 2: Analytical comparison between iono-free and ionospheric-affected PSDs (a) and time-domain chip shaping (b) for a wideband BOC modulation, i.e., BOC(50,50) carried at $f_0 = 1176.45$ MHz, with a TEC = 10 TECu. No receiver front-end, band-pass filter is considered.

(imaginary part in Fig. 2b is indeed null), both real and imaginary parts of the iono-affected signal now share the overall signal power due to the dispersive effect of the medium.
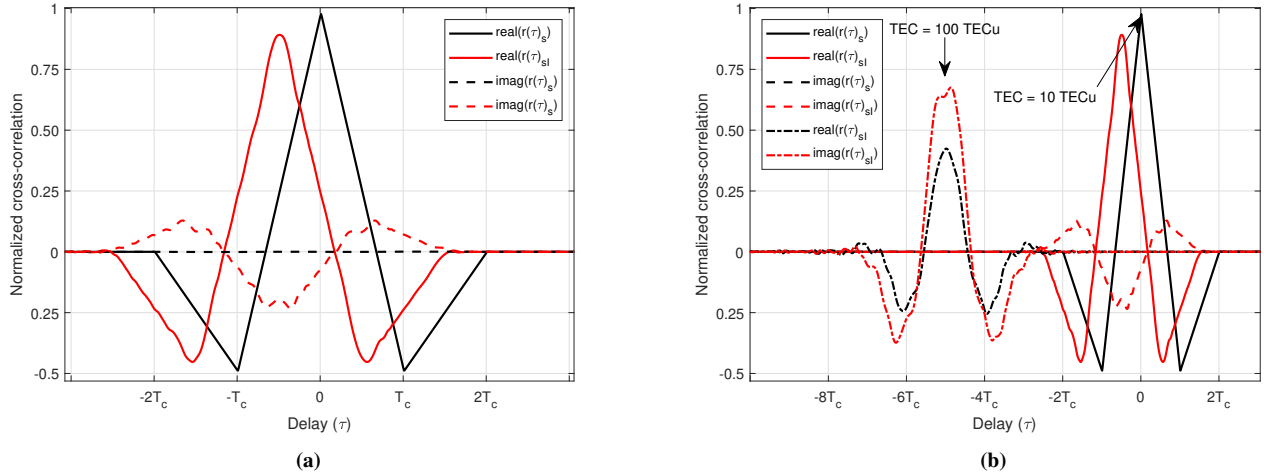

Figure 3: Effects of ionospheric group delay and phase advance on a BOC(50,50) carried at $f_0 =$ with a TEC = 10 TECu (a) and compared to the same chip shaping carried at the same carrier frequency with TEC = 100 TECu (b). No receiver front-end, band-pass filter is considered for this examples.

Fig. 3 shows the effect of both ionospheric group delay and phase advance on the correlation domain for different values of TEC. In Fig. 3a, we observe a time shift of the correlation peak due to a group delay of about $T_c/2$, affecting the correlation peak of the iono-affected signal. In continuity with the previous comments on the chip shape, we also observe that part of the energy is now transferred to the imaginary part of the correlation and that correlation peaks lost sharpness w.r.t. the signal autocorrelation. In Fig. 3b we compared the correlations of Fig. 3a with the emphasized effects on the same modulation scheme for TEC = 100 TECu. The plot shows a higher energy being transferred to the imaginary part and a non negligible loss of symmetry in the correlation peak.

III. METHODOLOGY

In contrast to existing literature on the topic (Gao et al., 2007; Zhao and Lei, 2023), our analysis of the correlation power loss induced by the ionosphere adopts a semi-analytical approach. This approach leverages the general definition of the Fourier transform of Multilevel Coded Spreading Symbols (MCSs), as introduced in (Ávila Rodríguez, 2008). We delve into the exploration of modulation schemes by utilizing this comprehensive expression for the Fourier transform of a multi-level subcarrier-modulated chip. The resulting spectral content is then conveyed at the chosen center frequencies, allowing us to investigate different operational bands through a subset of representative carrier frequencies.

Table 1: IEEE bands and representative center frequencies adopted in the current study.

IEEE/RNSS Band	IEEE frequency range	Repr. carrier frequency
L-Band E5a (Galileo) L5-Band (GPS)	1–2 GHz	1176.450 MHz
L-Band E5 (Galileo)	1–2 GHz	1191.795 MHz
L-Band E5b (Galileo)	1–2 GHz	1207.140 MHz
L2-Band (GPS)	1–2 GHz	1227.600 MHz
L-Band E6 (Galileo)	1–2 GHz	1278.750 MHz
L-Band Galileo E1/GPS L1/L1C/P(Y)/M-code	1–2 GHz	1575.420 MHz
S-Band	2–4 GHz	3.00 GHz
C-Band (Galileo reserved)	4–8 GHz	5.01 GHz
X-Band	8–12 GHz	10.00 GHz
Ku-Band	12–18 GHz	14.00 GHz
K-Band	18–27 GHz	22.50 GHz
K_a-Band	27–40 GHz	30.50 GHz

To limit the degrees of freedom of the investigation pursued within this study, we focused on a 100 MHz useful channel bandwidth. We regard this choice as a reasonable compromise between state-of-the-art signals leveraged by GNSS and proposals for wideband signals in LEO. A 128 MHz null-to-null bandwidth of the transmitted channel has been considered to provide a reasonable margin, which, when combined with the useful bandwidth, maintains a comparable ratio to that used for Galileo E1 (Julien and Issler, 2008). Our analysis primarily focuses on comparing wideband and narrowband signals regarding their performance when affected by dispersive ionospheric impairments. In view of this, we specifically selected a baseline BPSK modulation to represent the wideband signal. As for the narrowband case study, we conducted a comparative evaluation involving high-order BOCs and meta-signals. The latter can be considered narrowband to some extent, depending, essentially, on their chip rates and frequency separation of the main lobes.

1. Signal design and analysis

A reference BPSK(50) was selected as a simplistic reference modulation to fit the pre-defined wideband channel. The signal was defined in frequency domain through (1), by assuming $s_1 = 1$ and $R_c = 50 \cdot 1.023$ Mcps.

a) Bandwidth-equivalent BOC and meta-signals

We select a set of frequency spacing $\Delta f \in (50, 60, 68, 80, 90, 92, 96, 98)$ MHz. We also defined a set of chip rates, $R_c \in (25, 20, 17, 10, 5, 4, 2, 1)$ Mcps such that $\Delta f/2 + R_c = 50$ MHz is kept constant throughout the experiments. The net result is that, whether $\Delta f/2$ is used as subcarrier rate of a BOC modulation or as half frequency separation between the two signal component of a meta-signal, by satisfying this constraint we keep the main lobes of the narrowband signal under test within a band of 100 MHz.

In order to design a meta-signal we adopt two adjacent BPSK signals with given, identical chip rates R_c and with a frequency spacing Δf. Fig. 4 shows the PSD of the signals considered for the current study with different sample values of

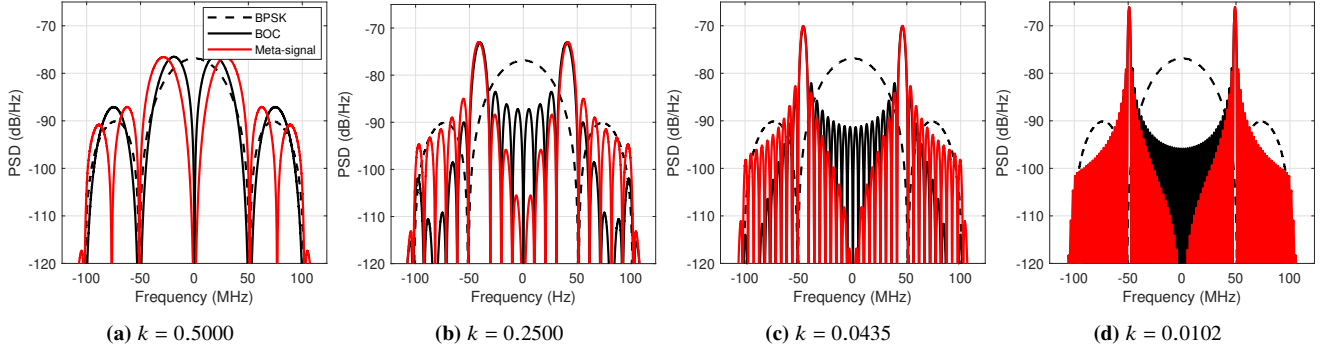$$k = \frac{R_c}{\Delta f} \ . \tag{6}$$

Figure 4: PSDs of the subcarrier modulations under analysis by varying the design parameter k.

It is worth noticing that for small values of k the Gabor bandwidth is increased and the central portion of the channel can host a further signal component by leveraging the low spectral densities of both BOC-modulated signals and meta-signal. This may be of interest for combining communication channel and radionavigation signals. Furthermore, in this specific spectral region meta-signals typically show a lower power density than BOC-modulated signals, thus limiting inter-channel interference in case of hybrid solutions.

b) Front-end and Ionospheric filtering

By avoiding numerical signal generation, we started from the frequency-domain definition of the signals of interest. We hence assume to get the Fourier transform, $S(f)$, of a generic discrete-time, real-valued subcarrier sequence s_i where $i = 1, ..., n$. In detail, we obtain the $S(f)$ for BPSK, BOC and Meta-signal modulation schemes through (1).

Then, we limit the bandwidth of the transmitted signal by emulating a payload front-end Infinite Impulse Response (IIR) filter with transfer function $H_F(f)$ such that

$$S_F(f) = S(f)H_F \tag{7}$$

The front-end filter settings have been established by assuming a useful bandwidth according to (Julien and Issler, 2008). The order of the filter was $N = 9$ with a pass-band frequency of 128 MHz. Passband ripples have been constrained to 0.01 dB and the stop-band attenuation was set to 80 dB. We then apply the phase term induced by the ionosphere by performing a further filtering of the signal in the frequency domain through (2)

$$S_I(f) = S_F(f)H_I(f) = S_F(f)e^{-j2\pi f \tau(f, \text{TEC})/c} \tag{8}$$

In order to compute the autocorrelation function we switch to the time domain through the inverse Fourier transform, by computing

$$s_I(t) = \mathscr{F}^{-1}(S_I(f)) \tag{9}$$

We then compare the autocorrelation function of the time domain signal and the cross-correlation function of the signal and the ionospheric-affected signal. We eventually compute a peak search of the correlation peaks and we estimate the power loss as

$$L_I = 10 \log_{10} \left[\max(R(t)) / \max(R_I(t)) \right] \tag{10}$$

Fig. 5 shows a block diagram which summarizes the aforementioned methodology for the two branches we identified as i) iono-free and ii) iono-affected processing branches. On the right branch we perform the aforementioned step to characterize iono-affected signals while on the left we follow a basic chain that does not include ionospheric filtering. The simulation environment was set to explore the following degrees of freedom

- TEC values included in the range 1–300 TECu, with a granularity of 1 TECu

- frequency band, investigated with representative carrier frequencies, captured in Tab. 1

- different design of bandwidth-equivalent BOC and meta-signal, by varying the parameter k

2. Experimental analysis

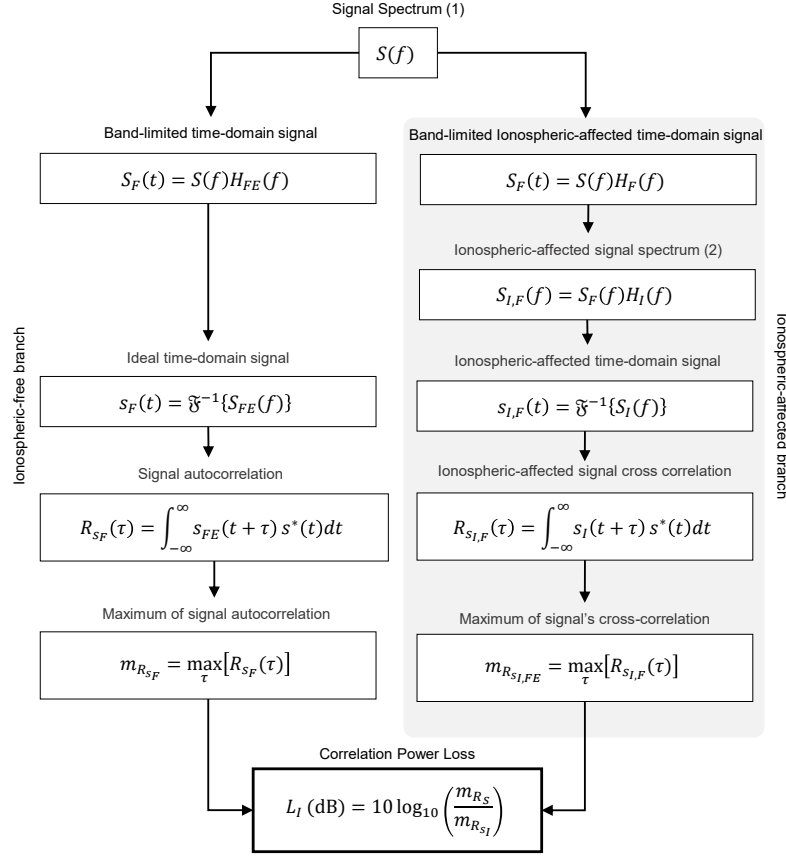The analysis has been performed addressing three different tasks which are detailed in the following.

Signal Spectrum (1)

$$S(f)$$

Band-limited time-domain signal

$$S_F(t) = S(f)H_{FE}(f)$$

Band-limited Ionospheric-affected time-domain signal

$$S_F(t) = S(f)H_F(f)$$

Ionospheric-affected signal spectrum (2)

$$S_{I,F}(f) = S_F(f)H_I(f)$$

Ideal time-domain signal

$$s_F(t) = \mathfrak{F}^{-1}\{S_{FE}(f)\}$$

Ionospheric-affected time-domain signal

$$s_{I,F}(t) = \mathfrak{F}^{-1}\{S_I(f)\}$$

Signal autocorrelation

$$R_{S_F}(\tau) = \int_{-\infty}^{\infty} s_{FE}(t+\tau)\, s^*(t)\,dt$$

Ionospheric-affected signal cross correlation

$$R_{S_{I,F}}(\tau) = \int_{-\infty}^{\infty} s_I(t+\tau)\, s^*(t)\,dt$$

Maximum of signal autocorrelation

$$m_{R_{S_F}} = \max_\tau\big[R_{S_F}(\tau)\big]$$

Maximum of signal's cross-correlation

$$m_{R_{S_{I,FE}}} = \max_\tau\big[R_{S_{I,F}}(\tau)\big]$$

Correlation Power Loss

$$L_I \text{ (dB)} = 10\log_{10}\left(\frac{m_{R_S}}{m_{R_{S_I}}}\right)$$

Ionospheric-free branch

Ionospheric-affected branch

Figure 5: Block diagram of the proposed methodology to quantify the correlation loss on transionospheric signals. Flow-chart and methodology inspired by (Gao et al., 2007).

a) Analysis of the correlation power loss vs TEC

A first analysis looks at the behaviour of the different modulation schemes in terms of correlation power loss by varying the TEC. Furthermore, the analysis is performed for the different bands of interest (see Tab. 1) to appreciate the lower impact of the ionospheric phase advance at higher frequencies but still to emphasize the advantage of the proposed meta-signal design.

Once advantages have been observed for some specific values of k, it is of interest to observe the correlation power loss by varying the design parameter k for BOC-modulated signals and meta-signals.

b) Analysis of the correlation power loss varying the design parameter k

The second set of results shows the optimal combination for designing a BPSK meta-signal which can be more robust than both BOC and BPSK signals to the ionopsheric phase advance while observing the similarities and difference between meta-signals and BOC-modulated signals w.r.t. the design paramater k. In this experiment we are comparing sets of signals that are constrained to the same nominal channel bandwidth occupation in terms of main spectra lobes. This condition is referred to as *bandwidth-equivalence* for BOC and meta-signals.

c) Analysis of the correlation power loss varying the design parameter k, assuming infinite-bandwidth signals

This last analysis generalizes the previous one by providing a more exhaustive view on the effects of the ionospheric channel when further spectral components are considered. To achieve the results of this investigation, the signals have been designed over a bandwidth equal to $500 \cdot 1.023\,\text{MHz}$, thus observing their spectral components in the interval $\pm250\,\text{GHz}$.

IV. RESULTS

1. Correlation power loss varying TEC

Fig. 6 shows the behaviour of the correlation loss varying the TEC at different sample carrier frequencies. In each figure, the correlation power loss of meta-signals is represented by a solid line with star markers, while triangles indicate the BOC counterpart. BPSK results are depicted by dashed lines. Overall, we observe that meta-signal shows the lowest correlation power loss in the lower bands while BPSK is the overall best at higher frequency bands. However, accounting for the y-axis scale, it is worth noticing that at higher frequencies the three signals behave very similarly. The sharp loss fluctuations of BOC and meta-signals are indeed of fractions of dB. Although they are mostly visible in the aforementioned upper bands, such periodic fluctuations still follow an increasing trend which has been highlighted in the literature (Gao et al., 2007) up to 1000 TECu.

By referring to the lower L-Band, in Fig. 6a to Fig. 6e we notice that the most relevant advantage in terms of robustness to dispersive medium is obtained by the meta-signal for TEC $\in$ (150, 300) TECu. L1-band, in Fig. 6f shows an increasing divergence of BOC and meta-signal curves with TEC, that highlight a growing robustness of the latter at higher TEC values. Similarly, at S-band (Fig. 6g), we still observe a positive divergence with a slight advantage of the meta-signals for high TEC values. However, the correlation power-loss reaches 0.01 dB for the BOC modulation and about 0.0075 dB for the meta-signal.
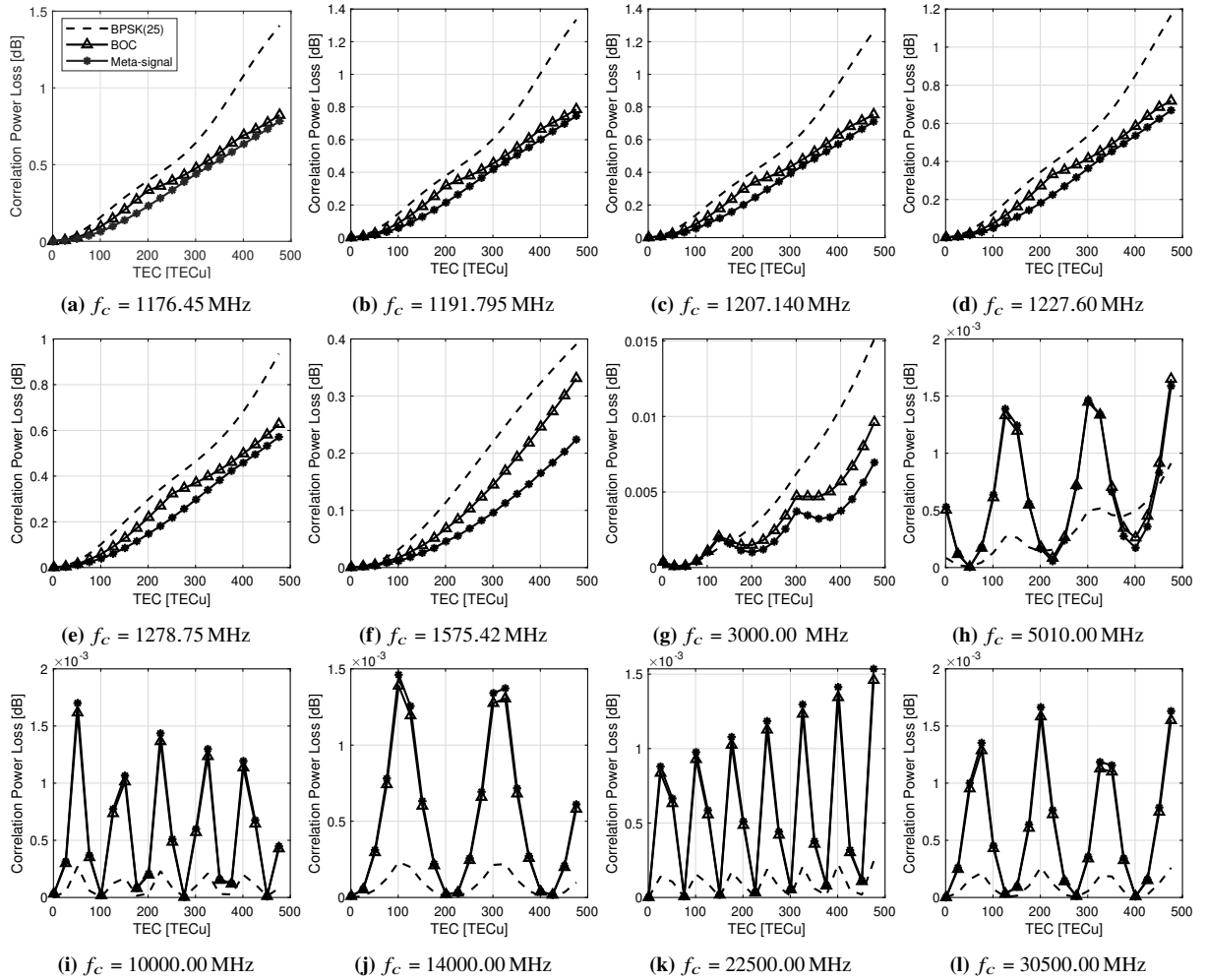

(a) f_c = 1176.45 MHz **(b)** f_c = 1191.795 MHz **(c)** f_c = 1207.140 MHz **(d)** f_c = 1227.60 MHz

(e) f_c = 1278.75 MHz **(f)** f_c = 1575.42 MHz **(g)** f_c = 3000.00 MHz **(h)** f_c = 5010.00 MHz

(i) f_c = 10000.00 MHz **(j)** f_c = 14000.00 MHz **(k)** f_c = 22500.00 MHz **(l)** f_c = 30500.00 MHz

Figure 6: Correlation power loss experienced by BPSK(25), BOC(50,50) and BPSK-based meta-signals. Finite bandwidth signals for $k = 0.0435$. Scales on y-axes are not homogeneous to highlight minimal variations and differences.

2. Correlation power loss varying the design parameter k

The results presented in the following figures compare the trend of correlation power loss for BOC and bandwidth-equivalent BPSK meta-signals, organized by frequency bands. The performance of BPSK does not depend on k. Although some

peculiarities may be observed in the different plots, the correlation power loss typically increases with the TEC, shown from left to right on the rows. This trend is emphasized by the BPSK curves, that are consistent with the correlation loss levels shown in the corresponding plots of Fig. 6. As a general trend, BPSK meta-signals provide lower losses than bandwidth-equivalent BOC modulations in most of the examples.

In the lower L-band and for small k, from Fig. 7 to Fig. 11, similar behaviors of the curves are observed, indicating that both BOC and meta-signals consistently experience lower loss compared to BPSK modulation. Additionally, the correlation power loss of meta-signals provides an advantage over BOC curves for small k that is lost for greater values. This advantage is attributed to the limited power density contained between the main lobes of the meta-signal power spectral density, which becomes more significant as k decreases in comparison to BOC. In Fig. 12, the observed trends are preserved, and a general reduction in loss is experienced by the entire set of signals, attributed to the higher carrier frequency used.

By moving to IEEE S-Band, the trends are mutated. In Fig. 13, we observe a higher correlation power loss of BOC and meta-signals w.r.t. the BPSK, for low TEC values, i.e. Fig. 13a and Fig. 13b, while lower values appears for higher TEC values, thus denoting the advantage observed for L-Band. Performance divergence between BOC and meta-signal is less regular than in lower bands but still shows the advantage of meta-signals at higher TEC.

In C-Band we observe similar losses for BOC, meta-signals and BPSK modulation, although a increasing trend is still visible with k and with the TEC values as well. However, for $k > 0.1$ BOC and meta-signals correlation power loss are higher than the BPSK. This worsening is confirmed for the higher frequency bands although is anticipated to values of k that are closer to 0.
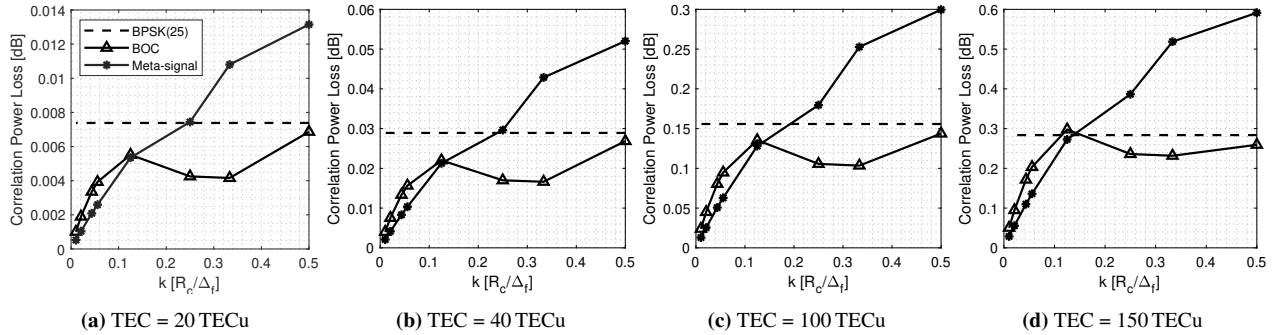

(a) TEC = 20 TECu   **(b)** TEC = 40 TECu   **(c)** TEC = 100 TECu   **(d)** TEC = 150 TECu

Figure 7: L-Band E5a (Galileo) L5-Band (GPS); f_c = 1176.45 MHz.

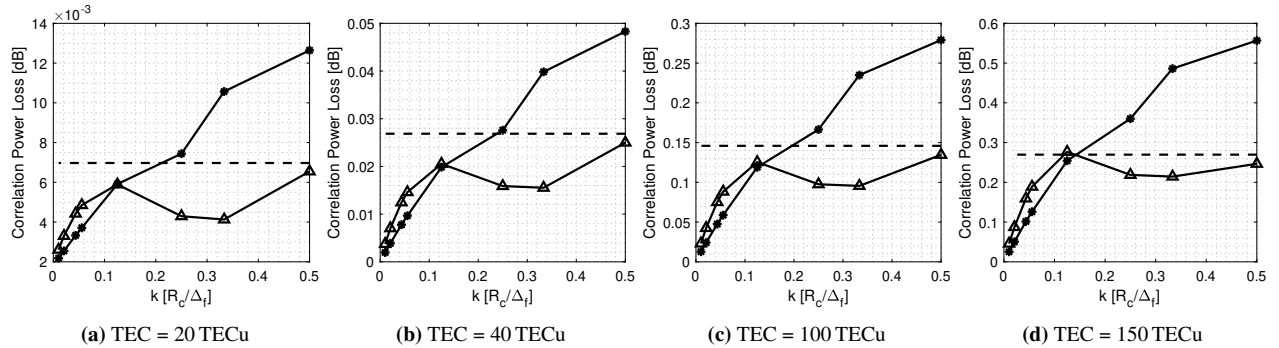**(a)** TEC = 20 TECu   **(b)** TEC = 40 TECu   **(c)** TEC = 100 TECu   **(d)** TEC = 150 TECu

Figure 8: L-Band E5 (Galileo); f_c = 1191.795 MHz

3. Infinite bandwidth signal: The detrimental effects of sidelobes in BOC

It comes natural to inspect the behaviour of the proposed signals while extending the observable signal bandwidth to emulate an infinite bandwidth signal reception. Although this condition may sounds unrealistic for real receivers, this analysis provides a glimpse on the true potential of wideband meta-signals in case they can be received by wideband receiver front-end.

As we can notice from the examples in Fig. 19 meta-signals show the higher robustness to the phase effect for any band and any value of TEC, also becoming steadily more robust than BPSK and bandwidth-equivalent BOC for almost any value of k. In parallel BOC modulations suffer due to the presence of more powerful spectral components that samples the phase response
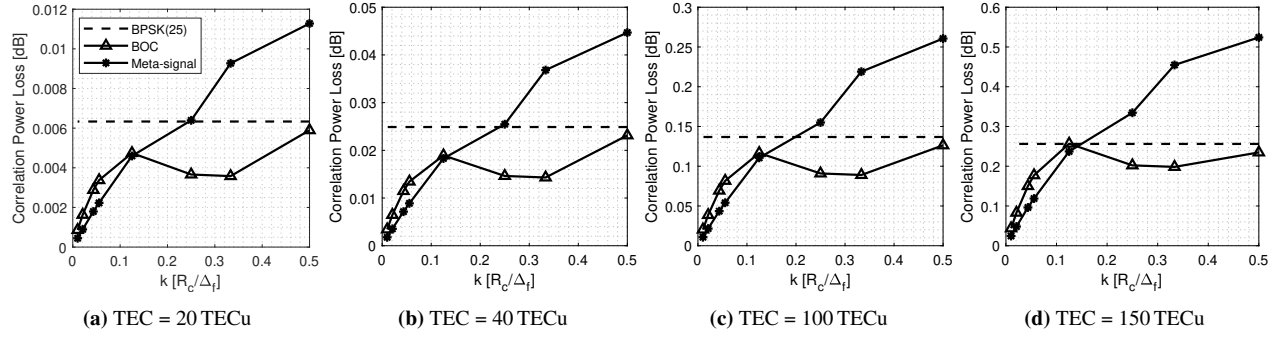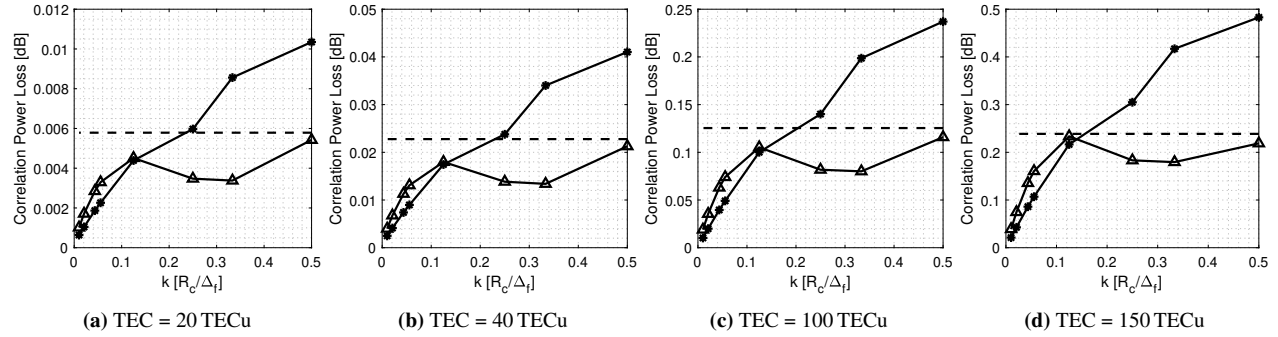
Figure 9: L-Band E5b (Galileo); $f_c = 1207.140$ MHz.
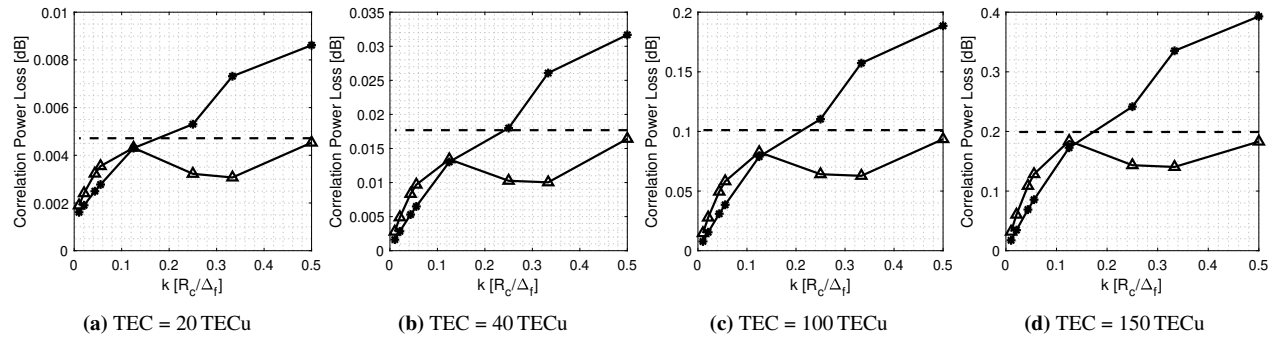

Figure 10: L2-Band (GPS); $f_c = 1227.60$ MHz.

Figure 11: L-Band E6 (Galileo); $f_c = 1278.75$ MHz.
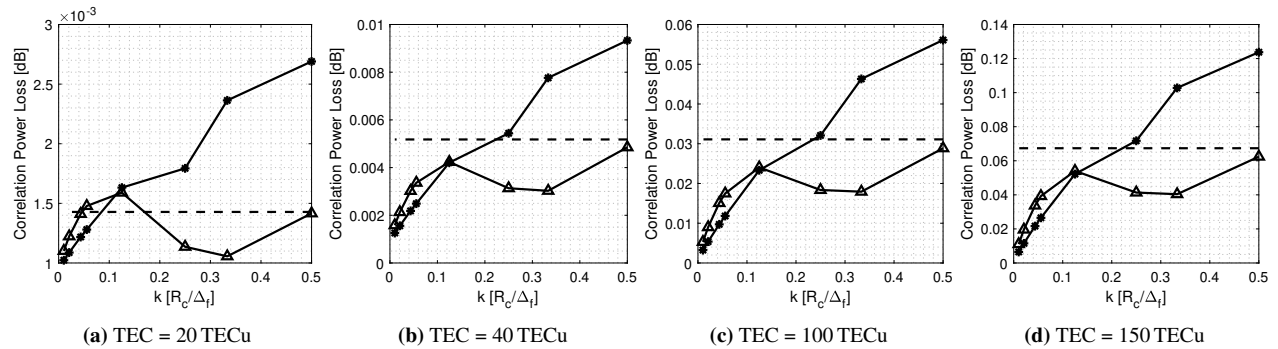

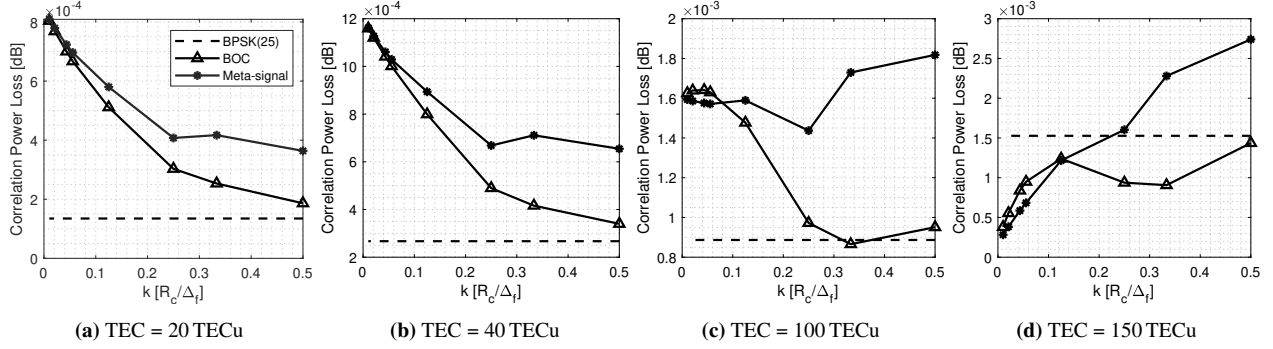**Figure 12:** L-Band Galileo E1/GPS L1/L1C/P(Y)/M-code; $f_c = 1575.42$ MHz.

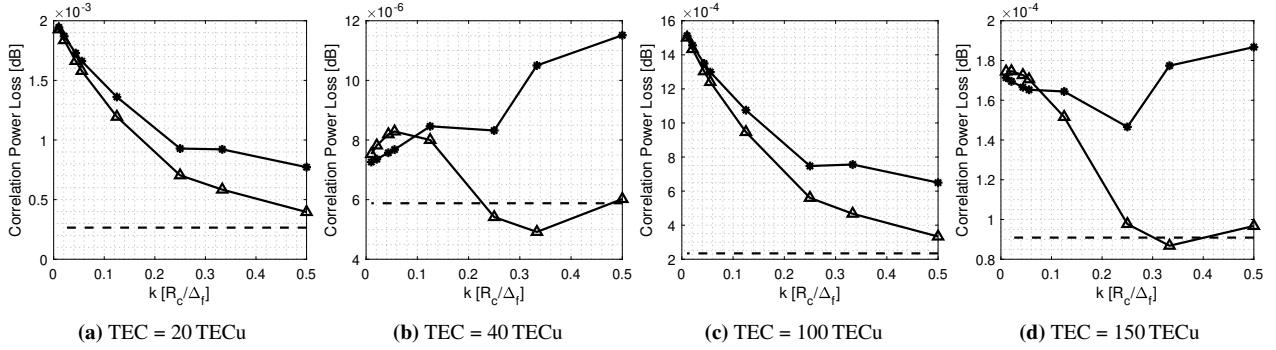**Figure 13:** IEEE S-Band; f_c = 3000.00 MHz; Finite bandwidth signal

Figure 14: IEEE C-Band (Galileo reserved); f_c = 5010.00 MHz; Finite bandwidth signal
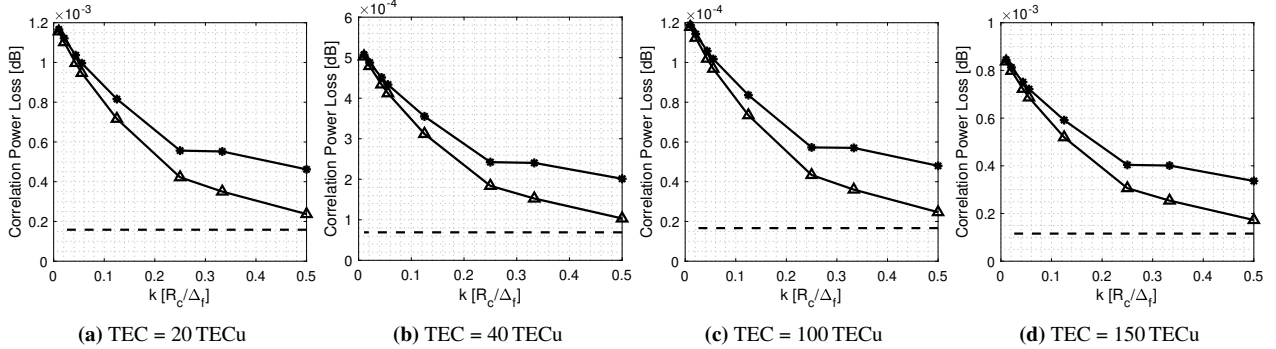

Figure 15: IEEE X-Band; f_c = 10000.00 MHz; Finite bandwidth signal

of the dispersive channels on a wider bandwidth. As an example we selected a subset of results for TEC=100 TECu. It can be shown that despite of specific magnitude variations, the trend of the correlation power loss is preserved for any TEC value.

V. CONCLUSIONS

Wideband transionospheric radionavigation signals may suffer from non-negligible dispersive nature of the ionosphere. The magnitude of the effect is dominated by the TEC. Phase advance causes correlation power loss at the receiver which is as remarkable as the signal spectral components include powerful sidelobes falling in the channel bandwidth.

High-order BOC modulations typically carry a large number of non-negligible sidelobes which contribute to the overall correlation power loss as they are affected by sever ionospheric delay gradient.

As a preliminary conclusion and in line with early literature findings, this study proposes to consider replacing wideband and ultra-wideband radio-navigation signals with bandwidth-equivalent meta-signals in LEO PNT to take advantage on their
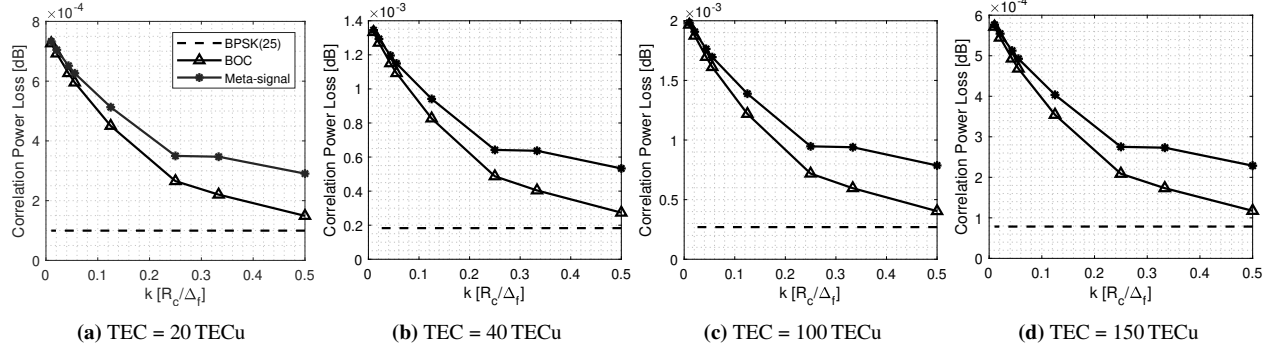
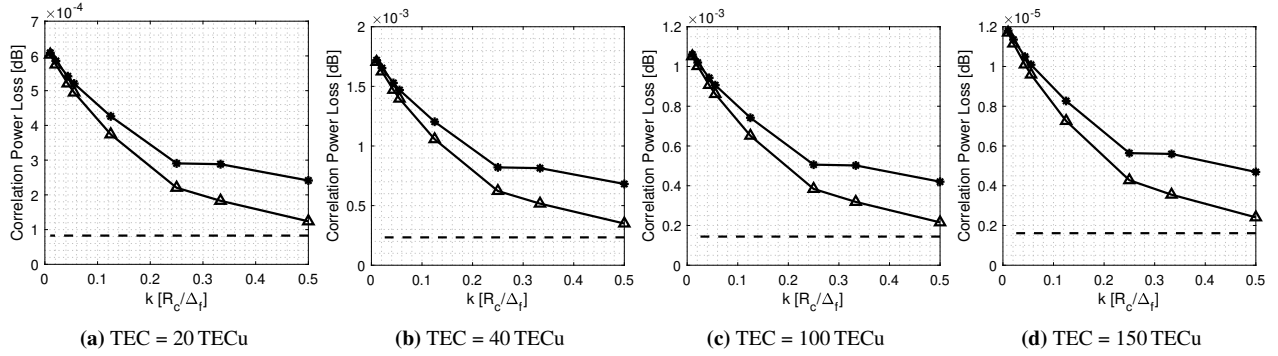**Figure 16:** IEEE Ku-Band; f_c = 14000.00 MHz; Finite bandwidth signal

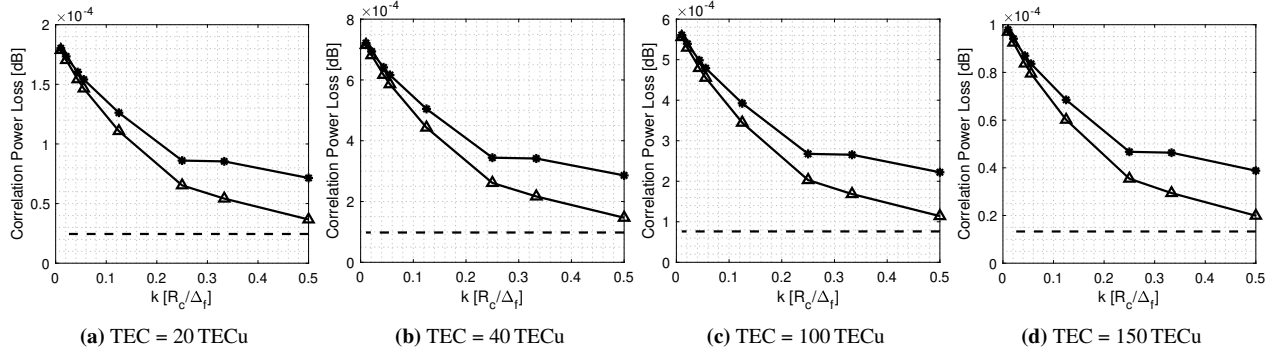**Figure 17:** IEEE K-Band; f_c = 22500.00 MHz; Finite bandwidth signal

Figure 18: IEEE Ka-Band; f_c = 30500.00 MHz; Finite bandwidth signal

features while keeping similar or better performance w.r.t. BOC modulations. By harnessing the power of meta-signals, we aim to support the use of advanced modulation schemes that can in turn enable high-accuracy LEO PNT and contribute to the development of more robust and accurate global positioning systems for the near future.

The sample results collected in this demonstrate that meta-signals show a good resilience to phase advance and efficient exploitation of wideband and ultra-wideband portions of the LEO PNT dedicated Radio Frequency (RF) spectrum. In detail, well-designed meta-signals show limited ionospheric-induced phase distortion while preserving the advantages of high Gabor Bandwidth modulation schemes.

ACKNOWLEDGEMENTS
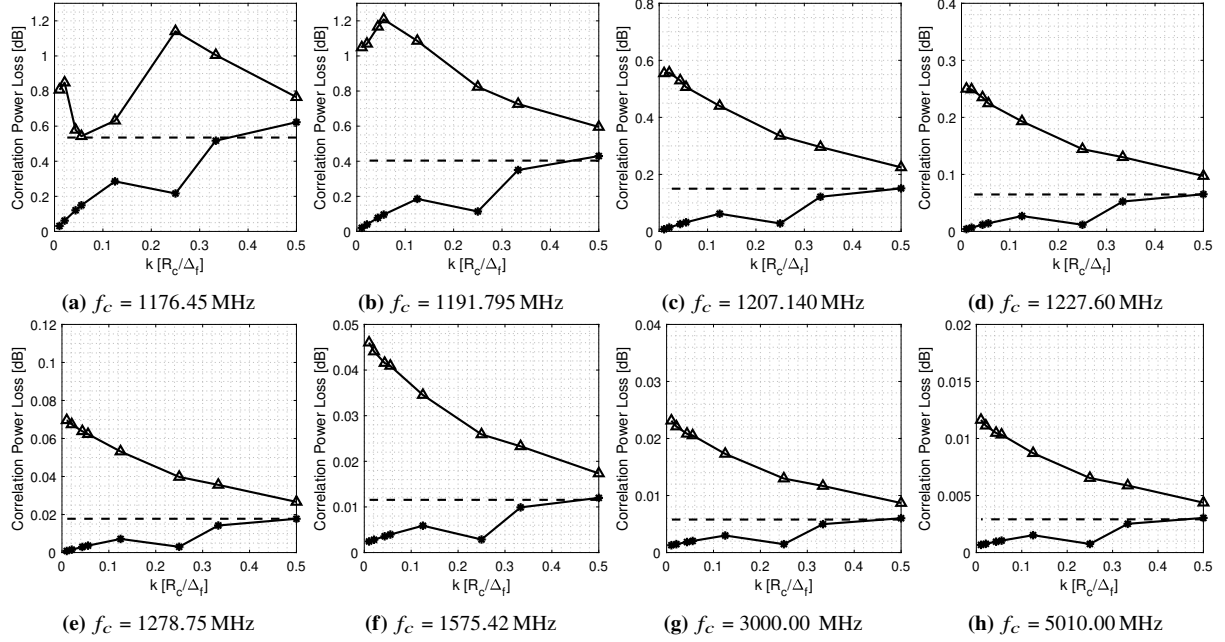
Figure 19: Correlation power loss experienced for infinite bandwidth signals with TEC= 100 TECu.

The subfigure captions are:
(a) $f_c = 1176.45\,\text{MHz}$ **(b)** $f_c = 1191.795\,\text{MHz}$ **(c)** $f_c = 1207.140\,\text{MHz}$ **(d)** $f_c = 1227.60\,\text{MHz}$
(e) $f_c = 1278.75\,\text{MHz}$ **(f)** $f_c = 1575.42\,\text{MHz}$ **(g)** $f_c = 3000.00\,\text{MHz}$ **(h)** $f_c = 5010.00\,\text{MHz}$

nor the European Commission can be considered responsible for them.

The authors acknowledge Thales Alenia Space Italy for the technical discussions on the topic and the invaluable insights.

REFERENCES

Ávila Rodríguez, J. Á. (2008). *On generalized signal waveforms for satellite navigation*. PhD thesis, München, Univ. der Bundeswehr, Diss., 2008.

Borio, D. and Gioia, C. (2023). Reconstructing GNSS meta-signal observations using sideband measurements. *NAVIGATION: Journal of the Institute of Navigation*, 70(1).

Chang, N., Hong, X., Wang, W., and Seco-Granados, G. (2022). A GNSS meta-signal SAGE-based multipath-mitigating loop design. *Digital Signal Processing*, 131:103759.

Diessongo, H. T., Bock, H., SCHÜLER, T., JUNKER, S., and KIROE, A. (2012). Exploiting the Galileo E5 wideband signal. *Inside GNSS*, 7(5):64–73.

Egea-Roca, D., López-Salcedo, J. A., Seco-Granados, G., and Falletti, E. (2021). Comparison of several signal designs based on chirp spread spectrum (CSS) modulation for a LEO PNT system. In *Proceedings of the 34th International Technical Meeting of the Satellite Division of The Institute of Navigation (ION GNSS+ 2021)*, pages 2804–2818.

Gao, G. X., Datta-Barua, S., Walter, T., and Enge, P. (2007). Ionosphere effects for wideband GNSS signals. In *Proceedings of the 63rd Annual Meeting of The Institute of Navigation (2007)*, pages 147–155.

Gao, Y., Yao, Z., and Lu, M. (2020). High-precision unambiguous tracking technique for BDS B1 wideband composite signal. *Navigation*, 67(3):633–650.

García-Molina, J., Lapin, I., Plakidis, E., Cordero, M., Sarnadas, R., Caparra, G., Karpf, M., Parro, J., Vazquez, C., Budianu, A., et al. (2023). Multi-layer pnt solutions for harsh user conditions. In *Proceedings of the 36th International Technical Meeting of the Satellite Division of The Institute of Navigation (ION GNSS+ 2023)*, pages 1587–1597.

Hoque, M., Jakowski, N., and Berdermann, J. (2017). Transionospheric microwave propagation: Higher-order effects up to 100 GHz. *Intech Open Science Open Minds: London, UK*, pages 15–38.

Hoque, M. M. and Jakowski, N. (2012). Ionospheric propagation effects on GNSS signals and new correction approaches. *Global navigation satellite systems: signal, theory and applications*, pages 381–405.

Imel, D. A. (1994). Evaluation of the TOPEX/POSEIDON dual-frequency ionosphere correction. *Journal of Geophysical Research: Oceans*, 99(C12):24895–24906.

Ji, J., Liu, Y., Chen, W., Wu, D., Lu, H., and Zhang, J. (2021). A novel signal design and performance analysis in navcom based on leo constellation. *Sensors*, 21(24):8235.

Julien, O. and Issler, J.-L. (2008). Compatibility of galileo e1 signals with the radio-astronomy band 9. In *GNSS SIGNAL 2008, 3rd Workshop on GALILEO Signals and Signal Processing*.

Kindervatter, T. H. and Teixeira, F. L. (2022). *Tropospheric and Ionospheric Effects on Global Navigation Satellite Systems*. John Wiley & Sons.

Nardin, A., Dovis, F., and Fraire, J. A. (2020a). Empowering the tracking performance of LEO PNT by means of meta-signals. In *2020 IEEE International Conference on Wireless for Space and Extreme Environments (WiSEE)*, pages 153–158. IEEE.

Nardin, A., Dovis, F., and Fraire, J. A. (2021). Empowering the tracking performance of LEO-based positioning by means of meta-signals. *IEEE Journal of Radio Frequency Identification*, 5(3):244–253.

Nardin, A., Dovis, F., and Motella, B. (2020b). Impact of non-idealities on GNSS meta-signals processing. In *2020 European Navigation Conference (ENC)*, pages 1–8. IEEE.

Paonni, M., Curran, J. T., Bavaro, M., and Fortuny-Guasch, J. (2014). GNSS meta signals: Coherently composite processing of multiple GNSS signals. In *Proceedings of the 27th International Technical Meeting of the Satellite Division of The Institute of Navigation (ION GNSS+ 2014)*, pages 2592–2601.

Perevalova, N. P., Afraimovich, E. L., Voeykov, S. V., and Zhivetiev, I. V. (2008). Parameters of large-scale TEC disturbances during the strong magnetic storm on 29 october 2003. *Journal of Geophysical Research: Space Physics*, 113(A3).

Pireaux, S., Defraigne, P., Wauters, L., Bergeot, N., Baire, Q., and Bruyninx, C. (2010). Higher-order ionospheric effects in GPS time and frequency transfer. *GPS solutions*, 14:267–277.

Ries, L., Limon, M. C., Grec, F.-C., Anghileri, M., Prieto-Cerdeira, R., Abel, F., Miguez, J., Perello-Gisbert, J. V., D'Addio, S., Ioannidis, R., Ostillio, A., Rapisarda, M., Sarnadas, R., and Testani, P. (2023). LEO-PNT for augmenting Europe's space-based PNT capabilities. In *2023 IEEE/ION Position, Location and Navigation Symposium (PLANS)*, pages 329–337.

Ya'acob, N., Tajudin, N., Remly, M. S. A., Ali, D. M., Sarnin, S. S., and Naim, N. F. (2019). Observation of ionosphere scintillation and total electron content (TEC) characteristic at equatorial region. In *Journal of Physics: Conference Series*, volume 1152, pages 1–7. IOP Publishing.

Zhao, D. and Lei, Y. (2023). Effects of ionosphere dispersion on wideband GNSS signals. *Frontiers in Physics*, 11:95.